Published in final edited form as:
J Control Release. 2017 March 10; 249: 53–62. doi:10.1016/j.jconrel.2016.12.045.

Murine Ultrasound-Guided Transabdominal Para-Aortic Injections of Self-Assembling Type I Collagen Oligomers

Alexa A. Yrineo[1,+], **Amelia R. Adelsperger**[1,+], **Abigail C. Durkes**[2], **Matthew R. Distasi**[3], **Sherry L. Voytik-Harbin**[1,4], **Michael P. Murphy**[3,5], and **Craig J. Goergen**[1,6,*]

[1]Weldon School of Biomedical Engineering, Purdue University, West Lafayette, Indiana, United States of America

[2]Department of Comparative Pathobiology, Purdue University, West Lafayette, Indiana, United States of America

[3]IU Health Center for Aortic Disease/Department of Surgery, Indiana University School of Medicine, Indianapolis, Indiana, United States of America

[4]Department of Basic Medical Sciences, Purdue University, West Lafayette, Indiana, United States of America

[5]Richard L. Roudebush VA Medical Center, Indianapolis, Indiana, United States of America

[6]Center for Cancer Research, Purdue University, West Lafayette, Indiana, United States of America

Abstract

Abdominal aortic aneurysms (AAAs) represent a potentially life-threatening condition that predominantly affects the infrarenal aorta. Several preclinical murine models that mimic the human condition have been developed and are now widely used to investigate AAA pathogenesis. Cell- or pharmaceutical-based therapeutics designed to prevent AAA expansion are currently being evaluated with these animal models, but more minimally invasive strategies for delivery could improve their clinical translation. The purpose of this study was to investigate the use of self-assembling type I collagen oligomers as an injectable therapeutic delivery vehicle in mice. Here we show the success and reliability of a para-aortic, ultrasound-guided technique for injecting quickly-polymerizing collagen oligomer solutions into mice to form a collagen-fibril matrix at body temperature. A commonly used infrarenal mouse AAA model was used to determine the target location of these collagen injections. Ultrasound-guided, closed-abdominal injections supported consistent delivery of collagen to the area surrounding the infrarenal abdominal aorta halfway between the right renal artery and aortic trifurcation into the iliac and tail arteries. This minimally invasive approach yielded outcomes similar to open-abdominal injections into the same region. Histological analysis on tissue removed on day 14 post-operatively showed

*Corresponding author: cgoergen@purdue.edu (CJG).
+Indicates authors contributed equally

minimal *in vivo* degradation of the self-assembled fibrillar collagen and the majority of implants experienced minimal inflammation and cell invasion, further confirming this material's potential as a method for delivering therapeutics. Finally, we showed that the typical length and position of this infrarenal AAA model was statistically similar to the length and targeted location of the injected collagen, increasing its feasibility as a localized therapeutic delivery vehicle. Future preclinical and clinical studies are needed to determine if specific therapeutics incorporated into the self-assembling type I collagen matrix described here can be delivered near the aorta and locally limit AAA expansion.

Graphical abstract

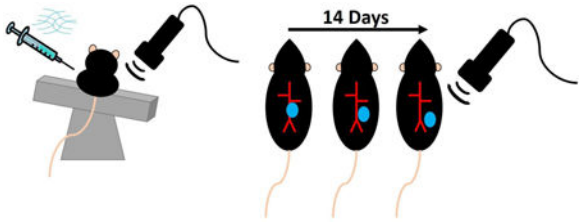

Introduction

Abdominal aortic aneurysms (AAAs) are pathological dilations of the aorta that are associated with significant morbidity and mortality (1), accounting for more than 150,000 deaths globally in 2013 (2). Several common murine AAA models have been developed that mimic many characteristics of the human condition. These include chemically-induced AAAs with either calcium chloride ($CaCl_2$) (3) or porcine pancreatic elastase (4,5), or genetically-induced in hyperlipidemic mice (6,7) infused systemically with angiotensin II (8–11). Current therapeutic strategies have focused on reducing extracellular matrix degradation and chronic inflammation (12,13), both of which are known to be important pathological features of AAAs (14). While most previous preclinical AAA work has administered experimental cell-based and pharmaceutical therapeutics through intraperitoneal injections (15), intravenous injections (16), or the animals' drinking water (17), minimally invasive injection strategies have the potential to locally deliver therapies with a clear translational potential (18).

Type I collagen is the major structural and mechanical determinant of the extracellular matrix within connective tissues (19,20). Due to its proteolytic degradability, biocompatibility, and low antigenicity, collagen has recently garnered interest as a clinically relevant biomaterial for therapeutic cell and molecule delivery (21). However, commercial grade monomeric collagen sources have slow polymerization rates and produce gels or matrices with low mechanical integrity, thus limiting their use as an injectable therapeutic delivery vehicle *in vivo* (22). Recently, a new soluble type I collagen subdomain, termed oligomers, has been isolated from porcine dermis (23). Oligomers uniquely retain their natural intermolecular crosslinks, which induce suprafibrillar self-assembly to yield highly-branched collagen-fibril networks with improved mechanical integrity (23). Specifically, oligomer matrices prepared at 0.5-4 mg mL^{-1} exhibit shear storage modulus (G') values of

40-1500 Pa compared to 2-300 Pa and 2-50 Pa for telocollagen and atelocollagen respectively (22). Oligomers also polymerize within minutes to form D-banded collagen-fibril materials with tunable properties, including fibril microstructure, matrix stiffness, and proteolytic degradation based on the polymerization parameters such as total collagen concentration and oligomer to monomer ratio (22,24,25). This previous work motivates further investigation of oligomers as an injectable self-assembling biomaterial for encapsulation and delivery of therapeutics *in vivo*.

Over the past 20 years, the field of image-guided interventions has greatly expanded by advances in medical imaging technology (26). With the real-time acquisition, portability, and low cost of ultrasound, it has emerged as an important imaging modality both in the clinic (27) and in preclinical animal research (28,29) for improved location, accuracy, precision, and overall success of image-guided injections. Without the aid of noninvasive imaging, delivery is typically limited to systemic injections that are commonly associated with off-target side effects in other organ systems (30–32) or open surgical implantation that is impractical with repeated treatments. Therapies delivered locally can potentially reduce these complications and target the aortic adventitia. Ultrasound guidance supports visualization of the target site and allows for minimally invasive delivery of therapies in both humans (33–35) and rodents (9,36–38).

In this study we describe a technique for murine para-aortic injections of self-assembling type I collagen oligomers with high frequency ultrasound guidance. Analysis of the success and reliability of these ultrasound-guided closed-abdominal injections are presented and compared to open injections after abdominal laparotomy. Here, success is defined as consistent localized delivery of the collagen volume midway between the right renal artery and aortic trifurcation into the iliac and tail arteries. Additionally, we present results of a longitudinal study designed to quantify the persistence and displacement of the formed collagen-fibril matrix *in vivo* over 14 days using high frequency ultrasound. Finally, we compare the length and target location of the collagen injection to the average length and position of an infrarenal AAA in a topical elastase mouse model (39). Our results suggest that injections of self-assembling oligomers via ultrasound guidance can be used as a minimally invasive delivery strategy within the peritoneal cavity of mice, specifically for the use as an infrarenal AAA therapeutic delivery vehicle. Future studies using this ultrasound-guided technique will be needed to determine if collagen encapsulated therapeutics can limit AAA expansion.

Materials and Methods

Topical Elastase AAA Disease Model

Animal Procedure—Wild-type male mice (n=9; 23.9 ± 1.4 g, 10.8 ±1.1 weeks old) from Harlan Laboratories (Indianapolis, IN) underwent laparotomies to induce infrarenal AAAs using a previously described topical elastase model (39). Briefly, we exposed the infrarenal aorta between the renal arteries and aortic trifurcation. Once exposed, a 4×2 mm piece of Gelfoam (Pharmacia & Upjohn Co., Pfizer Inc., New York, NY) was soaked in 50 μL type I porcine pancreatic elastase (3.6 mg/mL in water [with 0.01% thymol & trypsin at ≤50 BAEE units/mg protein], elastase activity measured to be between 27-34 units/mL, Sigma-Aldrich

Co., E1250, St. Louis, MO) was applied to the aorta for 10 minutes before being rinsed with 2 mL sterile saline. The animal was sutured closed, given a dose of carprofen (RIMADYL®, dose 5mg/kg, concentration 0.5mg/mL, amount 0.1mL/10g, Zoetis Inc., Kalamazoo, MI), and recovered. The Purdue Animal Care and Use Committee approved all procedures.

Ultrasound image collection and analysis—Ultrasound images were collected for each mouse before surgery and again at 3,7, and 14 days post-surgery. We collected B-mode and M-mode images of the infrarenal aorta in both long- and short-axis as well as short-axis 3D images. The images were analyzed using VevoLab software (FUJIFILM VisualSonics) to quantify length, diameter, and volume of the aneurysm over 14 days as well as vertical distance from the middle of the AAA to the iliac trifurcation. B-mode volumes were lofted together by manually drawing serial contours using parallel segmentation (0.57 mm or smaller step size). The first and last contours were used to determine aneurysm length. A linear distance measurement tool was used to determine the diameter and vertical distance.

Collagen Injections

Animal Use and Treatment—For this study, we used a total of 18 male C57BL/6 mice (32.0 ± 3.9 g, 18.8 ± 3.0 weeks old) from Harlan Laboratories (Indianapolis, IN) or bred at Purdue University (West Lafayette, IN). Six animals received ultrasound-guided closed-abdominal injections followed by euthanasia, six animals received open-abdominal injections followed by euthanasia, and six animals received ultrasound-guided closed-abdominal injections followed by 14 days of imaging surveillance with ultrasound. All animals were healthy prior to injection and body mass was monitored for the six recovered animals throughout the study. The Purdue Animal Care and Use Committee approved all procedures.

Type I Collagen Preparation—Type I collagen oligomers were derived from the dermis of domestic pigs and prepared as described previously (22). Prior to use, lyophilized collagen oligomers were dissolved in 0.01 N hydrochloric acid (HCl) and rendered aseptic by chloroform exposure at 4°C. A Sirius Red (Direct Red 80) assay was used to determine collagen concentration as previously described (40). The oligomer formulation was standardized based upon purity as well as polymerization potential according to the ASTM international consensus standard F3089-14 (41). Polymerization potential is defined by matrix shear storage modulus (G') as a function of collagen concentration of the polymerization reaction (22). The collagen solution was diluted with 0.01 N HCl and neutralized with both 10× phosphate buffered saline (PBS) and 0.1 N sodium hydroxide (NaOH) to achieve a pH of 7.4.

Oligomer polymerization kinetics were measured using an AR2000 rheometer (TA Instruments, New Castle, DE) equipped with a stainless-steel 40 mm-diameter parallel plate geometry. Upon lowering the geometry, the Peltier plate was maintained at 4°C for 5 minutes and then increased to 37°C for 15 minutes to induce collagen polymerization. Time-dependent changes in shear storage modulus (G') were measured at 1% controlled oscillatory strain. Polymerization half-time was calculated at the time at which G' equals half the maximum G' value (n=3). Cryo-SEM images displaying oligomer matrix

ultrastructure were obtained using an FEI NOVA nanoSEM 200 (FEI, Hillsboro, OR) varying between an Everhart-Thronley (<10,000× magnification) or immersion lens (>10,000× magnification) detector. Samples were quick frozen by submersion into critical point liquid nitrogen, transferred to a CT1000 col-stage attachment (Oxford Instruments North America, Inc., Concord, MA), and sublimated under vacuum for 15 minutes before sputter coating and imaging.

All oligomers were injected at a final collagen concentration of 2.1 mg/mL and volume of 150 μL, which yielded a 500 Pa collagen-fibril matrix. To visualize collagen following injection, blue food dye (Clover Valley, Dollar General Corporation, Goodlettsville, TN) was added to the PBS solution. Collagen solutions were kept on ice prior to injection, allowing for polymerization to occur once the solution warmed to body temperature (~37°C) post-injection.

Ultrasound-Guided Closed-Abdominal Injections

Animal Preparation—Transabdominal para-aortic injections were performed with ultrasound guidance in a total of 12 mice. Prior to imaging, animals were anesthetized in a 1 L induction chamber and kept unconscious with a coaxial nose cone non-rebreathing system that administered 1-3% isoflurane in 1.5 L/min medical grade air. Sterile eye lubricant was applied and animals were positioned on an adjustable heated stage set to 44°C to maintain internal body temperature near 37°C. Heart rate, respiration rate, and body temperature were monitored every 15 minutes with stage electrodes and a rectal probe, respectively. Hair on the ventral and dorsal sides was removed with clippers and depilatory cream (Nair, Church & Dwight Co., Inc. Ewing, NJ). Warm ultrasound transmission gel was applied liberally to the exposed skin prior to transducer placement.

Pre- and Post-Injection Imaging—For detection and monitoring of material injections, we used a high-resolution small animal ultrasound system (Vevo2100, FUJIFILM VisualSonics, Toronto, Canada) with a linear array transducer (MS550D, 256 elements, 40 MHz center frequency). Prior to injection, the right renal artery and aortic trifurcation were visualized in short axis on all animals positioned supine. To obtain animal-specific measurements, we used the y-axis stage controller to measure the length from the right renal artery to aortic trifurcation in millimeters. This total infrarenal aortic length was used to calculate a midpoint of the infrarenal aorta for each animal, the target location of our injection strategy. For baseline pre-injection ultrasound scans, transaxial three-dimensional B-mode images were acquired with respiration and cardiac gating from all animals (0.19 mm step size, 20 mm scan distance from the right renal artery to aortic trifurcation). Additionally, two-dimensional B-mode cine loops (100 frames) were acquired to the left and right of the infrarenal aorta in long axis. Similar three- and two-dimensional B-mode images were acquired on all animals post-injection and on the six recovered animals at days 1, 2, 3, 7, and 14 post-injection. The angle of the animal stage was adjusted for optimal aortic visualization and M-mode, color Doppler, and pulsed-wave Doppler acquisitions were used to discriminate arteries from veins.

Injection Procedure—Following baseline imaging, all animals were positioned prone and the stage was angled approximately 10° to the right. The transducer was clamped to an adjustable bench-mounted rail system, angled approximately 45° to the left, and positioned in a mediolateral orientation on all animals in short axis (Fig 1). The infrarenal aorta midpoint was visualized with B-mode and distinguished from the vena cava with M-mode and color Doppler. We adjusted the imaging depth between 10-11 mm to optimize aorta visualization.

An automated image-guided precision micro-injection system (FUJIFILM VisualSonics) was mounted to the left of the animal stage and used for all closed-abdominal injections. For accurate needle placement, an empty 1 mL syringe with a 27 G, ½ in. sterile needle was positioned in line with the transaxial plane of the transducer and angled approximately 45° downward parallel to the transducer (Fig 1). The injection mount controls were used to advance the needle directly under the transducer, requiring only minor adjustments of the transducer to enhance visualization of the needle tip in contact with the skin. Prior to breaking the skin surface, the trajectory of the needle was adjusted and visually aligned to ensure accurate placement with minimal injury. The needle was then inserted through the abdominal wall on the left side and positioned directly above the infrarenal aorta towards the animal's ventral side (Fig 2).

Following needle alignment, we loaded 150 μL of oligomer solution into a 1 mL syringe with a 27 G, ½ in. sterile needle that was pre-chilled in a -20°C freezer. The collagen filled syringe and needle were then clamped into the injection mount system with the bevel up, ensuring no adjustments were needed for alignment. We then inserted the needle tip directly above the infrarenal aorta and injected 150 μL of oligomeric collagen. A 440-500 frame B-mode cine loop was acquired both during injection and needle withdrawal for all para-aortic injections with a single focal zone on the aorta (S1 and S2 Videos). No para-aortic injections were performed on the right side of animals to serve as an internal control.

Conventional Open-Abdominal Injections

Animal Preparation—Para-aortic injections were performed in six mice without ultrasound guidance during an open-abdominal surgery approach. Animals were anesthetized and kept unconscious with isoflurane and medical grade air as mentioned above. A 50 W heating pad warmed to approximately 40°C was used to maintain internal body temperature at 37°C. The rate of respiration was monitored visually and the depth of anesthesia was assessed with periodic toe pinches. Aseptic technique was not followed for this non-recovery procedure, but hair on the ventral side was removed with depilatory cream.

Injection Procedure—The infrarenal aorta was surgically exposed and oligomeric collagen was prepared as described above. To mimic the closed-abdominal injections, the needle was manually guided through the abdomen from the left and positioned directly on top of the infrarenal aorta with the bevel down. Collagen was injected at the midpoint of the infrarenal aorta and a stereomicroscope (M60 with DFC290HD camera, Leica Microsystems, Wetzlar, Germany) was used to capture images before, during, and 5 minutes after the 150 μL para-aortic injection (Fig 3).

Animal Sacrifice and Dissection

We anesthetized all animals with isoflurane before euthanasia in a 1 L induction chamber with 0.2 L/min carbon dioxide following injection (n=12) or 14 days after recovery (n=6). The abdominal aorta from the suprarenal region down to the aortic trifurcation (including the kidneys, collagen injection, and all surrounding tissue) was carefully dissected and imaged with the same stereomicroscope. The abdominal tissue was fixed in 4% paraformaldehyde for 24 hours and then transferred to 0.1% paraformaldehyde for long-term storage. The spine was also removed from the fixed tissue prior to histological sectioning.

Histology Preparation and Staining

Fixed abdominal tissue at the target location (approximately 3 mm long and 20 mm wide) was dissected for sectioning. The tissues were oriented diagonally in single-chamber histology cassettes, held in place with foam biopsy pads, and stored in 0.1% paraformaldehyde until processing. The abdominal segments were then paraffin-embedded, thin-sectioned (5 μm), and adjacent sections were stained with hematoxylin and eosin (H&E) and Masson's trichrome (MTC) with an aniline blue staining kit (lot number 1528839, Newcomer Supply, Middleton, WI). The MTC stain was used to differentiate collagen (blue) from surrounding structures. We imaged stained tissue sections at both 10× and 40× magnification with a compound microscope (DM750 with ICC50W camera, Leica Microsystems).

Ultrasound Analysis and Validation

Post-injection ultrasound data was analyzed for days 0, 3, 7, and 14 with VevoLab software to quantify collagen implant dimensions (i.e. length, width, height) and volume. Both the vertical distance from the center of the collagen to the center of the infrarenal aorta and the closest horizontal distance from the aorta to the collagen were also measured to define implant displacement over the two-week period. B-mode volumes of collagen were segmented as mentioned above. The first and last contours were used to determine implanted collagen length. A linear distance measurement tool was used to determine the width, height, and displacement distances.

To validate the volume measurements, polyethylene tubing (PE50, Braintree Scientific, Braintree, MA) filled with oligomeric collagen was imaged with transaxial three-dimensional B-mode ultrasound (0.19 mm step size, 20 mm scan distance). The collagen volume was segmented manually by drawing serial contours and compared to the known volume calculated from the inner diameter and length of the tubing.

Dissection Image Analysis

Microscope images taken from dissection were analyzed with ImageJ software (42) to determine implanted collagen length, and horizontal and vertical collagen displacement distances from the infrarenal aorta. All images were accurately scaled prior to analysis and the straight line tool was used to measure distances.

Statistical Analysis

Data are represented as mean ± standard deviation (SD) and Minitab statistical software (Minitab, version 17) was used for all analysis. One-way ANOVA tests with post hoc Tukey comparisons were run to assess statistical significance of parameters between two time points or treatment groups. For all tests, we considered a p-value less than 0.05 to be significant.

Results

Oligomer exhibits rapid supramolecular self-assembly, transitioning from a solution to a continuous D-banded collagen-fibril scaffold

The fibrillar and suprafibrillar self-assembly displayed by type I collagen oligomers has the potential to provide the necessary microstructure and mechanical support for controlled drug, nanoparticle, or cell delivery. Since oligomers start as a viscous solution, they show excellent flowability even through small gauge needles, making them ideally suited for minimally invasive procedures. Upon warming body temperature (37°C), oligomers rapidly self-assemble with a polymerization half-time of 0.62±0.03 minutes as measured using a rheometer-based method. Ultrastructure analysis using cryo-SEM reveals that oligomers form a highly interconnected fibrillar scaffold with D-spacing patterns similar to those found within connective tissues *in vivo* (Figure 4).

Elastase AAA Develop Midway Between the Renal Arteries and Aortic Trifurcation

Using the collected ultrasound images, we found the average length of the AAAs to be 8.3 ± 1.13 mm over 14 days (Fig 5(e)). We also found that the average diameter (day 0: 0.66 ±0.05 mm, day 7: 0.97 ± 0.04 mm, day 14: 1.13 ± 0.13 mm) and volume (day 0: 2.31 ±0.40 mm^3, day 7: 5.08 ± 0.79 mm^3, day 14: 6.63 ± 1.37 mm^3) of these infrarenal aneurysms increased significantly from day 0 to day 14 ($p < 0.05$; Fig 5(a, b)). The average vertical distance from the middle of the AAAs to the start of the iliac arteries was 6.73 ± 1.18 mm (Fig 5(d)), which served as our target location for the collagen injection studies.

Ultrasound-Guided Injections Can Reliably Deliver Type I Collagen

For the closed-abdominal injections with (n=6) and without recovery (n=6), the midpoint of the infrarenal aorta and needle were easily distinguished in all animals and 92% (11 out of 12) of the injections could be visualized with ultrasound. We defined injection visualization as the formation of a growing hypoechoic region gradually separating the needle from the infrarenal aorta in synchrony with the injection of collagen. This formation caused the infrarenal aorta to shift, typically to the right and dorsally (S1 Video). Three-dimensional B-mode scans enabled us to visualize and analyze the hypoechoic implanted collagen and infrarenal aorta in all animals post-injection (S3 Video). Following injection on day 0, the collagen had a quantified mean volume of 45.2 ± 14.0 mm^3 that spanned a mean length of 9.0 ± 2.2 mm. Mean collagen width and height values were 5.3 ± 1.5 mm and 3.9 ± 1.0 mm, respectively. The mean horizontal distance between the collagen and the infrarenal aorta was 1.0 ± 0.8 mm, and the center of the collagen was, on average, 1.7 ± 0.9 mm distal to the center of the infrarenal aorta. To validate the volumetric ultrasound results, we measured the

polyethylene tubing (0.5842 mm inner diameter, 20 mm length) filled with oligomeric collagen to have an inner volume of 5.35 mm^3, which compared well with the known inner volume of 5.36 mm^3.

Ultrasound-Guided Closed-Abdominal Injections Are Similar to Open-Abdominal Injections

Measurements taken from dissection images showed no statistical differences between the collagen for the closed-abdominal and open-abdominal injections without recovery (Fig 6(a)). The mean length of the collagen implant was similar for both groups (closed-abdominal: 9.0 ± 0.7 mm and open-abdominal: 8.5 ± 3.0 mm, $p = 0.70$). We found that the collagen was slightly closer to the aorta in the open-abdominal group in the horizontal direction, but this did not reach statistical significance (closed-abdominal: 1.3 ± 1.3 mm and open-abdominal: 0.4 ± 0.6 mm, $p = 0.14$). Finally, the vertical displacement of the collagen's center towards the animal's tail from the infrarenal aorta's center was similar for both closed- and open-abdominal injections (closed-abdominal: 1.1 ± 0.3 mm and open-abdominal: 1.2 ± 0.9 mm, $p = 0.74$). Sample closed-abdominal and open-abdominal dissection images are shown in Figure 6(b, c).

Small Animal Ultrasound Enables Longitudinal Monitoring of Type I Collagen *In Vivo*

For the closed-abdominal injections with recovery, all six animals were fully ambulatory with no signs of complications. Average body mass went from 31 ± 4.1 g at day 0 pre-injection to 29 ± 3.2 g two days after injection, but then increased to 31 ± 2.4 g 14 days after injection. Three-dimensional B-mode scans on subsequent study days facilitated temporal monitoring of collagen injections (Fig 7). One of the animals had a substantial amount of abdominal gas at each time point, which prevented us from analyzing the ultrasound images, reducing the total number to five. Over the course of 14 days, the collagen volume (day 0: 49.5 ± 6.8 mm^3 to day 14: 51.8 ± mm^3, $p = 0.58$) did not change significantly (Fig 7(a)). The length (day 0: 7.9 ± 1.3 mm to day 14: 8.1 ± 0.9 mm, $p = 0.75$), width (day 0: 5.9 ± 1.3 mm^3 to day 14: 5.2 ± 0.5 mm^3, $p = 0.30$), and height (day 0: 3.7 ± 0.9 mm^3 to day 14: 4.5 ± 1.4 mm^3, $p = 0.30$) of the collagen also showed no significant difference over the 14-day period (Fig 7(b)). The collagen's distance from the aorta in both horizontal and vertical directions was also tracked, which indicated collagen implant displacement insignificantly leftward (1.1 ± 0.9 mm to 2.4 ± 1.0 mm, $p \leq 0.06$) and significantly distally (1.9 ± 0.6 mm to 3.9 ± 0.3 mm, $p \leq 0.001$) from the infrarenal aorta's center over 14 days (Fig 7(c)). Ultrasound measurements for recovery and non-recovery animals were compared to their respective dissection image measurements to further validate our method. Non-recovery group length (dissection: 9.0 ± 0.7 mm and ultrasound: 9.8 ± 2.5 mm, $p = 0.46$), horizontal displacement (1.3 ± 1.3 mm and 0.9 ± 0.8 mm, $p = 0.57$), and vertical displacement (1.1 ± 0.3 mm and 1.5 ± 1.1 mm, $p = 0.42$), as well as recovery group length (7.5 ± 1.9 mm and ± 0.9 mm, $p = 0.49$), horizontal displacement (1.5 ± 0.2 mm and 2.4 ± 1.0 mm, $p = 0.06$) were all found to be statistically similar for dissection image and ultrasound image analyses. The vertical displacement in the recovery group (1.9 ± 1.2 mm and 3.9 ± 0.3 mm, $p \leq 0.01$) was found to be statistically different between the dissection and ultrasound measurements. (Fig 8(a,b)). Representative ultrasound and dissection images from the closed-abdominal injections on days 0 and 14 are shown in Figure 8(c-f).

Histological cross-sections obtained on day 14 showed that the injected collagen was similar in appearance to the fibrillar collagen found in normal dense connective tissues (i.e., dermis). Leukocytes, mainly neutrophils, surrounded but did not invade the collagen implants at day 14 in the majority (5 out of 6) of recovery animals (Fig 9(a,b)). Only one recovery mouse had leukocytes infiltrating the injected collagen at day 14 (Fig 9(c,d)). Intralesional bacteria and focal collagen degradation were also observed to invade the collagen implant within this mouse.

Collagen Injection Location and Length Similar to AAA Model

We compared the location of the middle of the AAA to the middle of the collagen injections by measuring their respective distances above the iliac artery bifurcation (AAA: 6.73 ± 1.18 mm; collagen injection: 7.28 ± 0.38 mm) and found no statistically significant difference ($p = 0.15$; Fig 4(d)). When compared to the collagen implant, the average length (AAA: 8.30 ± 1.18 mm; collagen injection: 8.11 ± 0.88 mm) was also not significantly different ($p = 0.77$; Fig 4(e)).

Discussion

This work demonstrates utility of high frequency ultrasound for guidance and temporal monitoring of transabdominal para-aortic self-assembling type I collagen implants in mice. We showed that closed-abdominal injections with an ultrasound-guided technique delivered highly reproducible volumes of type I collagen oligomers to a target location near the infrarenal aorta. The outcomes of this minimally invasive approach, specifically reliable and reproducible volume delivery and localization, were similar to open-abdominal surgical injection strategy, showing our collagen could be placed similarly with ultrasound guidance without major surgery to administer a therapeutic.

Persistence of the injected collagen implant over a 14-day period was also documented with longitudinal ultrasound studies. The majority of recovery animals exhibited little to no cell invasion into the collagen implant, with one mouse showing more substantial leukocyte infiltration. Material persistence, together with the lack of significant cellular infiltration and minimized inflammatory response is especially noteworthy since conventional biologic-based injectables, including suspensions of decellularized tissue particulate or insoluble fibrillar collagens, are often associated with significant inflammatory/foreign body reactions and/or rapid degradation. These tissues responses are often characterized by dense infiltration of neutrophils, macrophages, and, in some cases, giant cells. Remnant cellular components (i.e., DNA) and/or extent of processing (i.e., exogenous crosslinking) have been implicated as the cause of these inflammatory/foreign body reactions (43). In contrast, oligomer collagen represents a highly purified formulation with defined molecular composition. This purified collagen, which is highly conserved across species (44), appears to eliminate many of the components known to induce adverse tissue responses and rapid degradation. Material sterilization, rather than aseptic preparation, and refinement of sterile injection may further assist in reducing overall inflammation in future studies. Taken together, these results suggest that this ultrasound-guided technique is an effective approach for delivery near the infrarenal aorta. Given this, further investigation will be needed to

determine if self-assembling type I collagen oligomers can be used as an injectable therapeutic delivery vehicle.

The infrarenal AAAs analyzed for this study showed a significant increase in the diameter and volume of the aorta midway between the renal and iliac arteries. This helped us identify our target for the collagen injections as 6.7 mm above the iliac bifurcation. The results of the collagen portion of this study revealed that we were able deposit an implant with a minimally invasive approach near the midpoint of the infrarenal aorta (the same location as the formation of the elastase-induced aneurysms). Furthermore, the comparable average lengths of the AAAs and the collagen implants showed that the polymerized collagen would be of adequate length to locally affect the entire AAA, not just a small region. Thus, this collagen injection technique could easily be paired in future studies with an infrarenal AAA model to test the efficacy and applicability of unproven controlled release therapeutics.

The clinical utility of para-aortic delivery of therapeutics via a trans-abdominal or trans-lumbar approach is significant, as others have noted (18). AAA is characterized by mural infiltration of cytotoxic T-cells, dendritic cells, and macrophages and current data suggests that it is the result of a dysregulated auto-immune response to a cryptic antigen(s). The resultant inflammatory cascade, with production of reactive oxygen species and proteases, leads to smooth muscle cell apoptosis and degradation of the extra-cellular matrix proteins. It is this latter process that leads to loss of the structural integrity of the aortic wall and pathological dilatation. A minimally invasive approach with ultrasound-guided placement of a needle through the lumbar muscles could deliver immunomodulatory cells, such as mesenchymal stromal cells or T regulatory cells, that can mitigate the inflammatory cell activity in its initiation (13). Intravenous delivery of cells results in significant pulmonary sequestration, as we have previously shown, whereas needle directed para-aortic delivery will concentrate cells near the aorta and may increase their potency (45).

When polymerized, type I collagen oligomers from porcine skin form an interconnected fibril network demonstrating mechanical integrity far exceeding that of conventional monomer collagen formulations (22). Previous work has shown that oligomeric collagen has tunable properties, including fibril microstructure, matrix stiffness, and proteolytic degradation, which are all known to influence cell fate (24,46). Kreger et al. showed that mesenchymal stem cells (MSCs) are able to sense and respond to the broad range of physical properties provided by collagen-fibril matrices and that these properties provide important guidance cues for fundamental MSC behavior *in vitro*, including lineage specific differentiation of MSCs *in vitro* (22). This suggests that the self-assembling collagen could be used as an effective *in vivo* delivery vehicle for MSCs while supporting modulation of fibril density and matrix stiffness. With their immunosuppressive activities, MSCs have been shown to improve the outcome of inflammation-based diseases such as aortic aneurysms by administration through tail-vein injections (13) and topical placement of MSC sheets (47), thus opening the door to investigate the translational potential of MSCs delivered with oligomeric collagen as a treatment strategy for AAAs. Future studies could also investigate oligomeric collagen as a localized delivery vessel for therapies such as microRNAs, monoclonal antibodies, and various small molecules for treating a variety of diseases

including cardiac remodeling (48), several cancers (49,50), diabetes (51), and Alzheimer's disease (52).

Despite the efficacy of our ultrasound-guided injections, some limitations in the present study remain. First, the presence of abdominal gas can disrupt ultrasound imaging. While some adjustment of the animal stage relative to the transducer can minimize this interference, this artifact sometimes remained unresolved and limited our ability to visualize the collagen implant. Optimal collagen visualization is crucial for accurate ultrasound analysis and a lack thereof could explain the difference between the polymerized collagen volume quantified (45.2 ± 14.0 mm^3) and the total collagen solution volume injected (150 mm^3). Another possible explanation for this volume discrepancy is the loss of interstitial fluid and compression of the formed collagen-fibril network upon injection within the confined tissue space. To better distinguish implanted collagen from surrounding structures, encapsulated gas-filled microbubbles could be used as a contrast agent, an approach that has become common in clinical imaging (53). Furthermore, compression of mice with the ultrasound probe could cause deformation of the collagen implant *in vivo*. Because of this, we made a strong effort to reduce the amount of pressure the transducer exerted on each mouse to diminish deformation. Finally, visualization of the injection, important for ensuring accurate collagen delivery, can be hindered by attenuation from the spine. We were able to visualize 92% (11 out of 12) of the closed-abdominal injections at the target site, suggesting that the spine did not create a major issue. In the one animal where the injection was not visualized with ultrasound, collagen was also not detected at the target location, suggesting inaccurate delivery. Because these injections are minimally invasive, an injection in future studies can always be repeated to ensure proper administration.

Conclusions

We demonstrated the utility of ultrasound-guided methods for successful and reliable delivery of self-assembling type I collagen oligomers to the region surrounding the infrarenal aorta in mice, based on a commonly used infrarenal AAA model. Our injected collagen implants had similar lengths as an infrarenal AAA and were delivered within close proximity to the aorta. In a longitudinal study, polymerized oligomer matrices persisted with insignificant proteolytic degradation and minimal inflammation and cell invasion over a two-week period. With advancements in tissue engineering and medical imaging, future studies could use this injection technique to develop and investigate novel therapeutics for AAAs and other diseases.

Supplementary Material

Refer to Web version on PubMed Central for supplementary material.

Acknowledgments

The authors gratefully acknowledge Clarissa Hernandez for her assistance with oligomeric collagen preparation and handling, Evan Phillips for guidance on the histology preparation, imaging, and analysis, and Gurneet Sangha for assistance with the polyethylene tube setup to validate ultrasound measurements. This work was supported in part to C.J.G. by the American Heart Association [grant 14SDG18220010] and the Purdue University Center for Cancer Research [Jim and Diann Robbers Cancer Research Grant for New Investigators]. It was also supported in part to

M.P.M. by Merit Review Award [CX001407] from the U.S. Department of Veterans Affairs CSRD, by the Indiana University Strategic Research Initiative, and by funds from the United States Department of Veterans Affairs through the Richard L. Roudebush VA Medical Center in Indianapolis, IN.

References

1. Hirsch AT, Haskal Z, Hertzer N, Bakal C, Creanger M, Halperin J, et al. ACC/AHA 2005 practice Guidelines for the Management of Patients With Peripheral Arterial Disease (Lower Extremity, Renal, Mesenteric, and Abdominal Aortic). Circulation. 2005; 113(11):1474–547.
2. Wang, H., Dwyer-Lindgren, L., Lofgren, K., Lozano, R., et al. Lancet. Vol. 385. Elsevier; 2015 Jan. Global, regional, and national age–sex specific all-cause and cause-specific mortality for 240 causes of death, 1990–2013: a systematic analysis for the Global Burden of Disease Study 2013; p. 117-71.
3. Chiou AC, Chiu B, Pearce WH. Murine aortic aneurysm produced by periarterial application of calcium chloride. J Surg Res. 2001 Aug; 99(2):371–6. [PubMed: 11469913]
4. Pyo R, Lee JK, Shipley JM, Curci JA, Mao D, Ziporin SJ, et al. Targeted gene disruption of matrix metalloproteinase-9 (gelatinase B) suppresses development of experimental abdominal aortic aneurysms. J Clin Invest. 2000 Jun; 105(11):1641–9. [PubMed: 10841523]
5. Bhamidipati CM, Mehta GS, Lu G, Moehle CW, Barbery C, DiMusto PD, et al. Development of a novel murine model of aortic aneurysms using peri-adventitial elastase. Surgery. 2012 Aug; 152(2): 238–46. [PubMed: 22828146]
6. Plump AS, Smith JD, Hayek T, Aalto-Setälä K, Walsh A, Verstuyft JG, et al. Severe hypercholesterolemia and atherosclerosis in apolipoprotein E-deficient mice created by homologous recombination in ES cells. Cell. 1992 Oct 16; 71(2):343–53. [PubMed: 1423598]
7. Zhang SH, Reddick RL, Piedrahita JA, Maeda N. Spontaneous hypercholesterolemia and arterial lesions in mice lacking apolipoprotein E. Science. 1992 Oct 16; 258(5081):468–71. [PubMed: 1411543]
8. Daugherty A, Manning MW, Cassis LA. Angiotensin II promotes atherosclerotic lesions and aneurysms in apolipoprotein E-deficient mice. J Clin Invest. 2000 Jun; 105(11):1605–12. [PubMed: 10841519]
9. Goergen CJ, Barr KN, Huynh DT, Eastham-Anderson JR, Choi G, Hedehus M, et al. In vivo quantification of murine aortic cyclic strain, motion, and curvature: implications for abdominal aortic aneurysm growth. J Magn Reson Imaging. 2010 Oct; 32(4):847–58. [PubMed: 20882615]
10. Goergen CJ, Azuma J, Barr KN, Magdefessel L, Kallop DY, Gogineni A, et al. Influences of aortic motion and curvature on vessel expansion in murine experimental aneurysms. Arterioscler Thromb Vasc Biol. 2011; 31(2):270–9. [PubMed: 21071686]
11. Phillips, EH., Yrineo, AA., Schroeder, HD., Wilson, KE., Cheng, JX., Goergen, CJ., et al. Biomed Res Int. Vol. 2015. Hindawi Publishing Corporation; 2015. Morphological and Biomechanical Differences in the Elastase and AngII *apoE* $^{-/-}$ Rodent Models of Abdominal Aortic Aneurysms; p. 1-12.
12. Maegdefessel L, Azuma J, Toh R, Merk DR, Deng A, Chin JT, et al. Inhibition of microRNA-29b reduces murine abdominal aortic aneurysm development. J Clin Invest. 2012 Feb; 122(2):497–506. [PubMed: 22269326]
13. Sharma AK, Lu G, Jester A, Johnston WF, Zhao Y, Hajzus VA, et al. Experimental abdominal aortic aneurysm formation is mediated by IL-17 and attenuated by mesenchymal stem cell treatment. Circulation. 2012 Sep 11; 126(11 Suppl 1):S38–45. [PubMed: 22965992]
14. Ailawadi G, Eliason J, Upchurch GJ. Current concepts in pathogenesis of abdominal aortic aneurysm. J Vasc Surg. 2003; 38(3):584–8. [PubMed: 12947280]
15. Kaneko H, Anzai T, Morisawa M, Kohno T, Nagai T, Anzai A, et al. Resveratrol prevents the development of abdominal aortic aneurysm through attenuation of inflammation, oxidative stress, and neovascularization. Atherosclerosis. 2011 Aug; 217(2):350–7. [PubMed: 21530968]
16. Fu X, Yamawaki-Ogata A, Oshima H, Ueda Y, Usui A, Narita Y. Intravenous administration of mesenchymal stem cells prevents angiotensin II-induced aortic aneurysm formation in apolipoprotein E-deficient mouse. J Transl Med. 2013; 11:175. [PubMed: 23875706]
17. Watanabe, A., Ichiki, T., Sankoda, C., Takahara, Y., Ikeda, J., Inoue, E., et al. Clin Sci (Lond). Vol. 126. Portland Press Limited; 2014 May. Suppression of abdominal aortic aneurysm formation by

inhibition of prolyl hydroxylase domain protein through attenuation of inflammation and extracellular matrix disruption; p. 671-8.

18. Baum, RA., Carpenter, JP., Golden, MA., Velazquez, OC., Clark, TWI., Stavropoulous, SW., et al. J Vasc Surg. Vol. 35. Elsevier; 2002 Jan. Treatment of type 2 endoleaks after endovascular repair of abdominal aortic aneurysms: Comparison of transarterial and translumbar techniques; p. 23-9.
19. Muiznieks LD, Keeley FW. Molecular assembly and mechanical properties of the extracellular matrix: A fibrous protein perspective. Biochim Biophys Acta - Mol Basis Dis. 2013; 1832(7):866–75.
20. Abou Neel EA, Bozec L, Knowles JC, Syed O, Mudera V, Day R, et al. Collagen — Emerging collagen based therapies hit the patient. Adv Drug Deliv Rev. 2013 Apr; 65(4):429–56. [PubMed: 22960357]
21. Friess W. Collagen--biomaterial for drug delivery. Eur J Pharm Biopharm Off J Arbeitsgemeinschaft fu r Pharm Verfahrenstechnik eV. 1998 Mar; 45(2):113–36.
22. Kreger ST, Bell BJ, Bailey J, Stites E, Kuske J, Waisner B, et al. Polymerization and matrix physical properties as important design considerations for soluble collagen formulations. Biopolymers. 2010 Aug; 93(8):690–707. [PubMed: 20235198]
23. Blum KM, Novak T, Watkins L, Neu CP, Wallace JM, Bart ZR, et al. Acellular and cellular high-density, collagen-fibril constructs with suprafibrillar organization. Biomater Sci. 2016 Apr 22; 4(4):711–23. [PubMed: 26902645]
24. Roeder BA, Kokini K, Sturgis JE, Robinson JP, Voytik-Harbin SL. Tensile mechanical properties of three-dimensional type I collagen extracellular matrices with varied microstructure. J Biomech Eng. 2002 Apr; 124(2):214–22. [PubMed: 12002131]
25. Whittington CF, Yoder MC, Voytik-Harbin SL. Collagen-polymer guidance of vessel network formation and stabilization by endothelial colony forming cells in vitro. Macromol Biosci. 2013 Sep; 13(9):1135–49. [PubMed: 23832790]
26. Cleary K, Peters TM. Image-guided interventions: technology review and clinical applications. Annu Rev Biomed Eng. 2010 Aug 15.12:119–42. [PubMed: 20415592]
27. Noble, JA., Navab, N., Becher, H., Tao, Z., Tagare, HD., Beaty, JD., et al. Interface Focus. Vol. 1. Royal Society; 2011 Aug 6. Ultrasonic image analysis and image-guided interventions; p. 673-85.
28. Springer ML, Sievers RE, Viswanathan MN, Yee MS, Foster E, Grossman W, et al. Closed-chest cell injections into mouse myocardium guided by high-resolution echocardiography. Am J Physiol Heart Circ Physiol. 2005 Sep; 289(3):H1307–14. [PubMed: 15908468]
29. Vázquez-Portalatín N, Breur GJ, Panitch A, Goergen CJ. Accuracy of ultrasound-guided intra-articular injections in guinea pig knees. Bone Joint Res. 2015; 4(1):1–5. [PubMed: 25588586]
30. Chollet, P., Favrot, MC., Hurbin, A., Coll, JL. J Gene Med. Vol. 4. John Wiley & Sons, Ltd; 2002 Jan. Side-effects of a systemic injection of linear polyethylenimine-DNA complexes; p. 84-91.
31. Brunetti-Pierri N, Palmer DJ, Beaudet AL, Carey KD, Finegold M, Ng P. Acute toxicity after high-dose systemic injection of helper-dependent adenoviral vectors into nonhuman primates. Hum Gene Ther. 2004 Jan; 15(1):35–46. [PubMed: 14965376]
32. Horneff G, Burmester GR, Emmrich F, Kalden JR. Treatment of rheumatoid arthritis with an anti-CD4 monoclonal antibody. Arthritis Rheum. 1991 Feb; 34(2):129–40. [PubMed: 1994909]
33. Sibbitt WL, Kettwich LG, Band PA, Chavez-Chiang NR, DeLea SL, Haseler LJ, et al. Does ultrasound guidance improve the outcomes of arthrocentesis and corticosteroid injection of the knee? Scand J Rheumatol. 2012 Feb; 41(1):66–72. [PubMed: 22103390]
34. Reach JS, Easley ME, Chuckpaiwong B, Nunley JA. Accuracy of ultrasound guided injections in the foot and ankle. Foot ankle Int. 2009 Mar; 30(3):239–42. [PubMed: 19321101]
35. Adler RS, Sofka CM. Percutaneous ultrasound-guided injections in the musculoskeletal system. Ultrasound Q. 2003 Mar; 19(1):3–12. [PubMed: 12970612]
36. Rodriguez-Porcel M, Gheysens O, Chen IY, Wu JC, Gambhir SS. Image-guided cardiac cell delivery using high-resolution small-animal ultrasound. Mol Ther. 2005 Dec; 12(6):1142–7. [PubMed: 16111921]
37. Abrahams D, Jeune-Smith Y, Bode A, Baldwin M, Choi JW. Real-time ultrasound-guided needle injection of the mouse jugular vein. Curr Protoc Mouse Biol. 2014; 4(3):141–50. [PubMed: 25723964]

38. Tuckett AZ, Zakrzewski JL, Li D, van den Brink MRM, Thornton RH. Free-hand Ultrasound Guidance Permits Safe and Efficient Minimally Invasive Intrathymic Injections in Both Young and Aged Mice. Ultrasound in Medicine & Biology. 2015; 41
39. Laser, A., Lu, G., Ghosh, A., Roelofs, K., McEvoy, B., DiMusto, P., et al. J Surg Res. Vol. 178. NIH Public Access; 2012 Dec. Differential gender-and species-specific formation of aneurysms using a novel method of inducing abdominal aortic aneurysms; p. 1038-45.
40. Brightman AO, Rajwa BP, Sturgis JE, McCallister ME, Robinson JP, Voytik-Harbin SL. Time-lapse confocal reflection microscopy of collagen fibrillogenesis and extracellular matrix assembly in vitro. Biopolymers. 2000 Sep; 54(3):222–34. [PubMed: 10861383]
41. ASTM F3089-14. Standard Guide for Characterization and Standardization of Polymerizable Collagen-Based Products and Associated Collagen-Cell Interactions. ASTM International; West Conshohocken, PA: 2014. www.astm.org
42. Schneider, CA., Rasband, WS., Eliceiri, KW. Nat Methods. Vol. 9. Nature Publishing Group; 2012 Jun 28. NIH Image to ImageJ: 25 years of image analysis; p. 671-5.
43. Badylak, SF., Gilbert, TW. Semin Immunol. Vol. 20. NIH Public Access; 2008 Apr. Immune response to biologic scaffold materials; p. 109-16.
44. Eyre DR, Paz MA, Gallop PM. Cross-linking in collagen and elastin. Annu Rev Biochem. 1984; 53:717–48. [PubMed: 6148038]
45. Xie J, Jones TJ, Feng D, Cook TG, Jester AA, Yi R, et al. Human Adipose-Derived Stem Cells Suppress Elastase-Induced Murine Abdominal Aortic Inflammation and Aneurysm Expansion Through Paracrine Factors. Cell Transplant. 2016
46. Voytik-Harbin, SL., Han, B. Collagen-Cell Interactions and Modeling in Microenvironments. In: Neu, CP., Genin, G., editors. CRC Handbook of Imaging in Biological Mechanics. Boca Raton, Florida: CRC Press and Taylor & Francis; 2015. p. 261-73.
47. Hashizume R, Yamawaki-Ogata A, Ueda Y, Wagner WR, Narita Y. Mesenchymal stem cells attenuate angiotensin II-induced aortic aneurysm growth in apolipoprotein E-deficient mice. J Vasc Surg. 2011 Dec; 54(6):1743–52. [PubMed: 21908146]
48. Buss NA, Henderson SJ, McFarlane M, Shenton JM, de Haan L. Monoclonal antibody therapeutics: history and future. Curr Opin Pharmacol. 2012; 12(5):615–22. [PubMed: 22920732]
49. Milne JC, Lambert PD, Schenk S, Carney DP, Smith JJ, Gagne DJ, et al. Small molecule activators of SIRT1 as therapeutics for the treatment of type 2 diabetes.
50. Nie, Q., Du, X., Geng, M. Acta Pharmacol Sin. Vol. 32. Nature Publishing Group; 2011 May 18. Small molecule inhibitors of amyloid β peptide aggregation as a potential therapeutic strategy for Alzheimer's disease; p. 545-51.
51. White AW, Westwell AD, Brahemi G. Protein – protein interactions as targets for small-molecule therapeutics in cancer.
52. Nicolaou S, Talsky A, Khashoggi K, Venu V. Ultrasound-guided interventional radiology in critical care. Crit Care Med. 2007 May; 35(5 Suppl):S186–97. [PubMed: 17446778]
53. Dindyal S, Kyriakides C. Ultrasound microbubble contrast and current clinical applications. Recent Pat Cardiovasc Drug Discov. 2011 Jan; 6(1):27–41. [PubMed: 21222650]

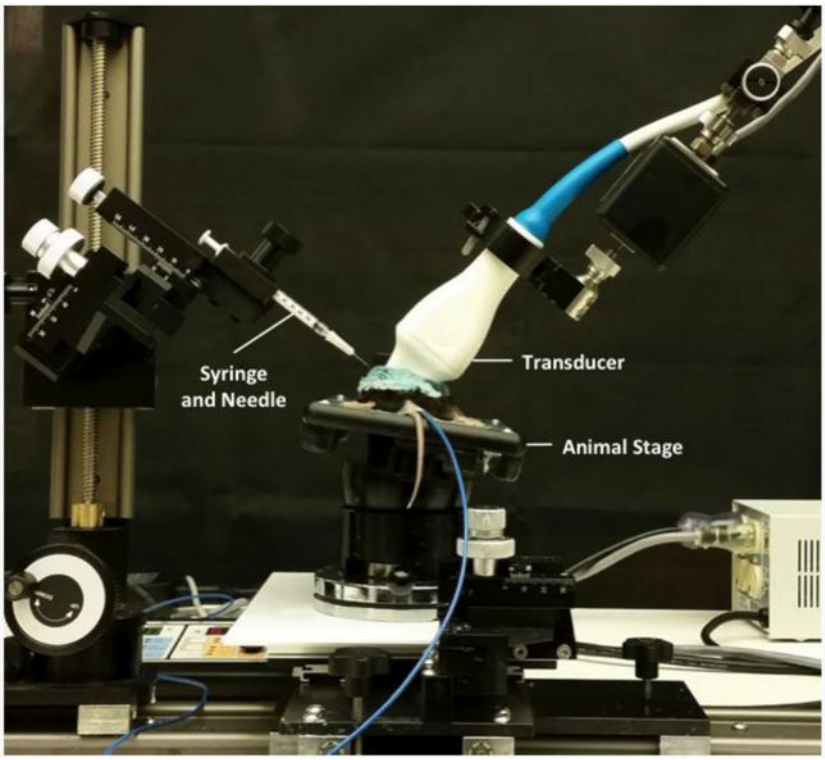

Fig 1. Set-up for ultrasound-guided closed-abdominal injections

An anesthetized mouse is shown on the animal stage. The ultrasound transducer as well as the syringe and needle are shown placed above the animal ready for injection.

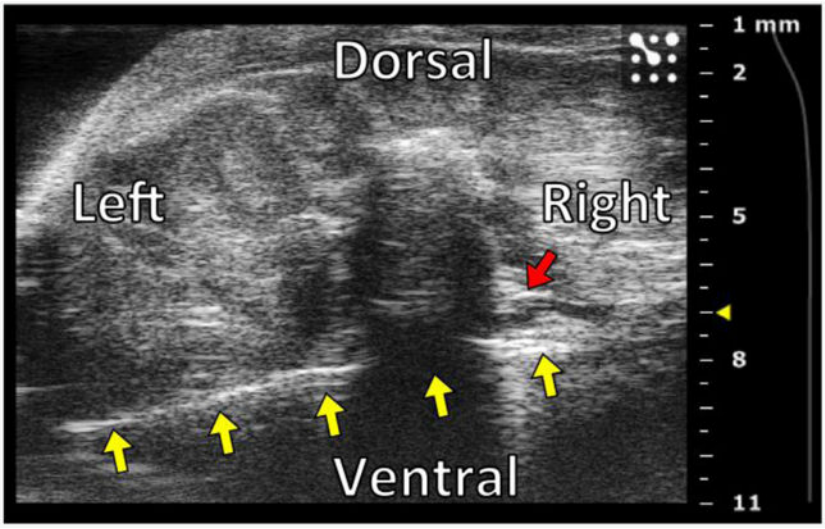

Fig 2. Ultrasound visualization of needle alignment in relation to infrarenal aorta pre-injection

Two-dimensional B-mode image in short axis showing the ultrasound-guided insertion of a 27 G needle (yellow arrows) through the abdomen and positioned directly above the infrarenal aorta (red arrow) towards the ventral side. The black shadow in the middle of the image represents signal attenuation from the spine. A single focal zone was set 7 mm deep at the injection target site.

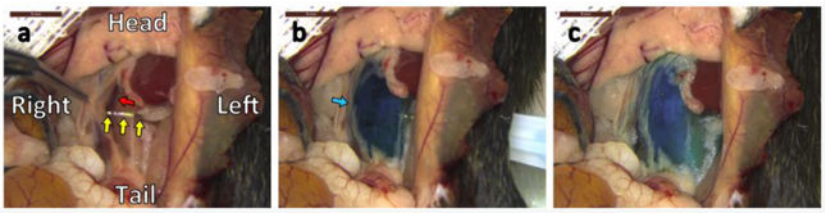

Fig 3. Open-abdominal injection of type I collagen during surgical procedure

Three stereomicroscope images show the surgical approach before (a), during (b), and 5 minutes after (c) an open-abdominal injection of oligomeric collagen (blue arrow). A 27 G needle (yellow arrows) with the bevel down was inserted through the abdomen from the left and positioned directly on top of the infrarenal aorta (red arrow). Scale bars = 5 mm.

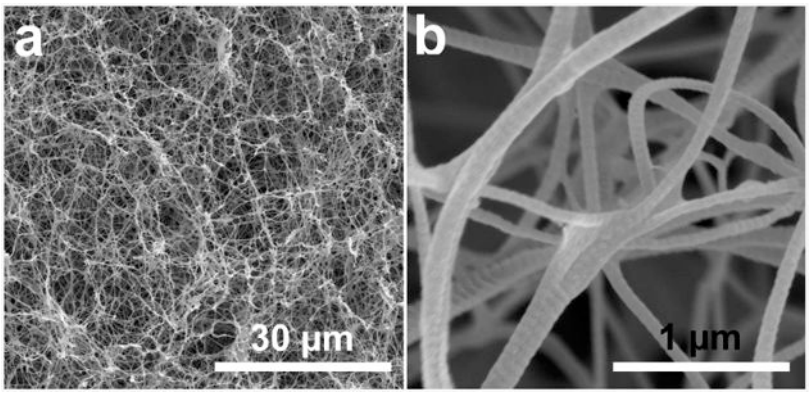

Fig 4. Type I collagen oligomers form highly interconnected fibrillar matrices

High resolution cryo-SEM images showing the type I collagen oligomers forming highly interconnected fibrillar matrices with D-periodic spacing similar to that found in connective tissues in vivo. Scale bars are 30 μm (a) and 1 μm (b), respectively.

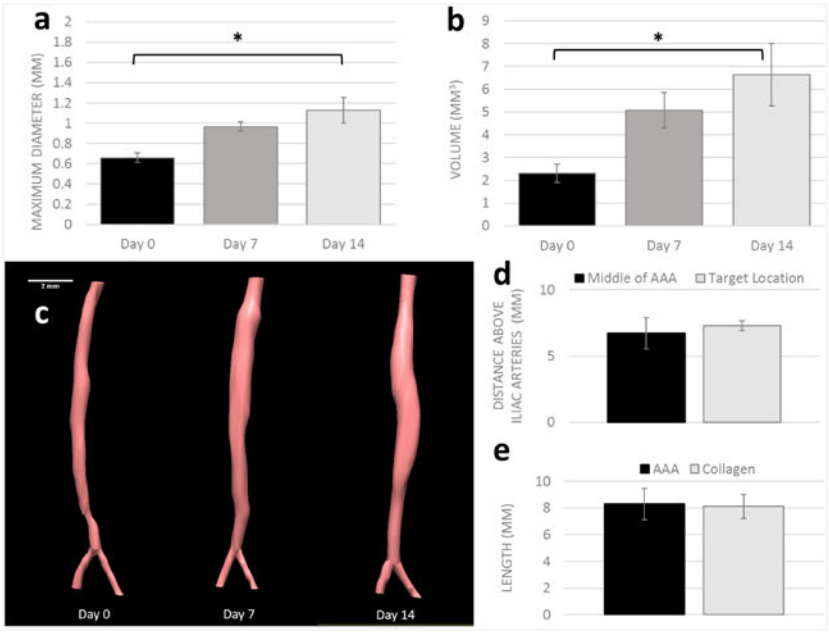

Fig 5. Infrarenal AAA Model Guides Collagen Injection Target

Mean ± SD for US measurements of AAA diameter (a) and volume (b) over 14 days. Example infrarenal AAA volume expansion is depicted over the same two weeks (c). Mean ± SD for comparisons between AAA and collagen implant length (d) as well as comparison between the distance above the iliac arteries for the middle of the AAA and the target of each collagen injection (e). Scale bars= 2 mm (c). * denotes statistical significance of AAA measurements between day 0 and 14 ($p < 0.05$).

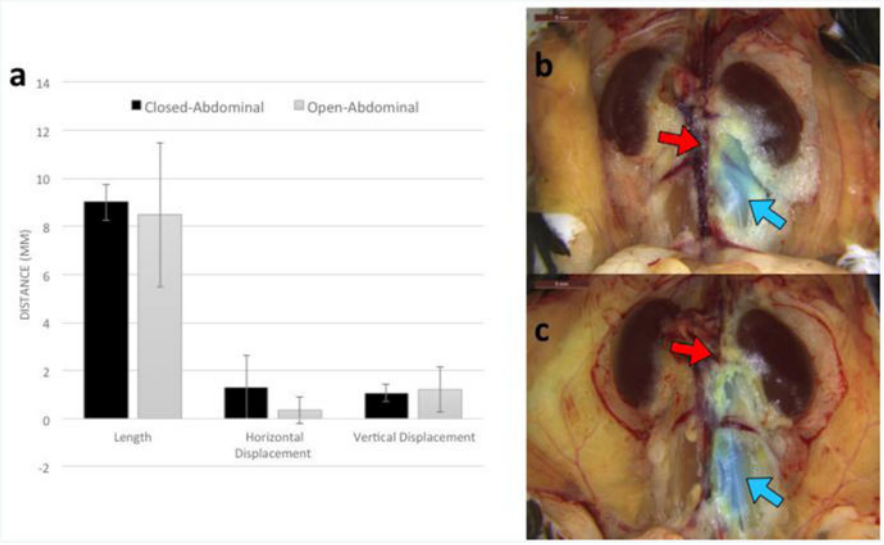

Fig 6. Comparison between closed-abdominal and open-abdominal injections

The mean ± SD (n=6) measurements for collagen, including implant length, and horizontal and vertical displacement from the aorta, were similar between closed-abdominal and open-abdominal injections in the non-recovery groups (a). No statistical differences between groups were observed (p-value range: 0.14-0.74). Representative closed-abdominal (b) and open-abdominal (c) dissection images show this similarity. Blue arrows point to the collagen, and red arrows point towards the infrarenal aorta. Scale bars = 0.5 mm.

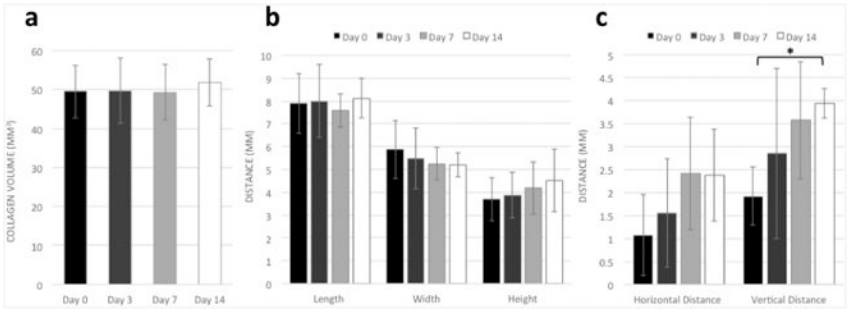

Fig 7. Type I collagen does not degrade significantly over 14 days *in vivo*

Mean ± SD measurements on days 0, 3, 7, and 14 (n=5) for collagen volume (a) and length, width, and height (b), as well as horizontal and vertical displacement distances (c). * denotes statistical significance of collagen measurements between day 0 and 14 ($p < 0.05$).

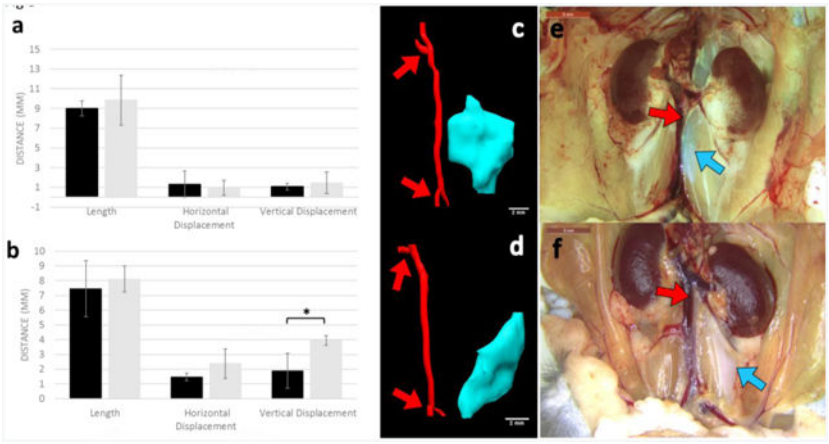

Fig 8. Type I collagen displacement over 14 days *in vivo* quantified through dissection and ultrasound image analysis

Mean ± SD measurements for dissection and ultrasound (US) image measurements of length, and horizontal and vertical displacements at end-point for non-recovery (a, n=6) and recovery (b, n=6) animals. Sample three-dimensional renderings for day 0 (c) and day 14 (d) showing the right renal artery (top arrow) and aortic trifurcation (bottom arrow) for reference points and leftward and distal shift of the collagen over two weeks *in vivo*. Example dissection images of collagen injection at day 0 (e) and day 14 (f) again emphasizing the collagen's shift leftward and distally (blue arrow) from the infrarenal aorta (red arrow). Scale bars = 2 mm (c,d) and 5 mm (e,f). * denotes statistical significance of collagen displacement measurements between day 0 and 14 ($p < 0.05$)

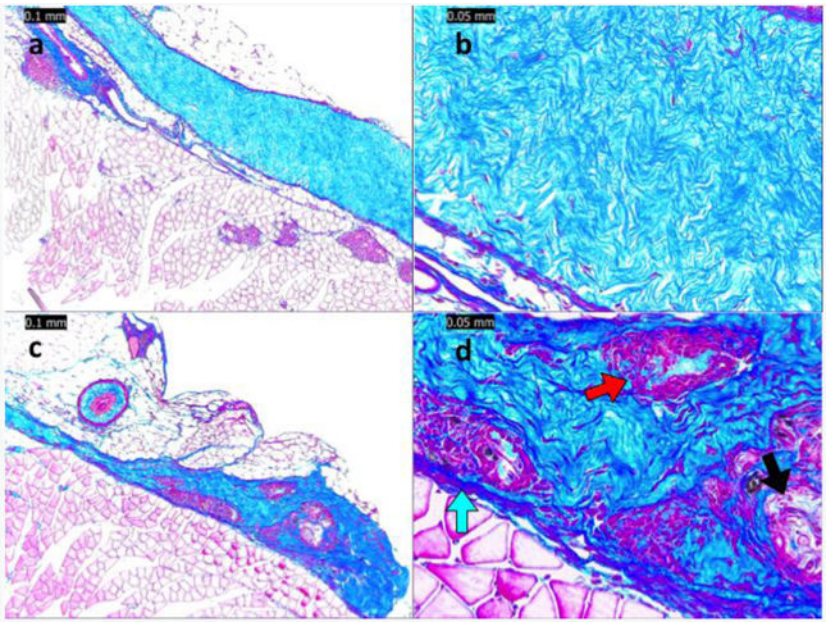

Fig 9. Representative histology images show range of leukocyte infiltrate at 14 days post-injection

MTC stained histology images depict representative cell infiltrate observed 14 days after collagen injection. The majority of collagen implants showed surrounding leukocytes with little to no cell invasion (a,b). One mouse showed leukocyte infiltration (blue arrow), bacteria aggregation (red arrow), and possible collagen degradation (black arrow) (c,d). Mild (a,b) and advanced (c,d) cell infiltrate are shown at 10× (a,c) and 40× times; (b,d) magnification. Scale bars = 0.1 mm (a,c) and 0.05 mm (b,d).